Journal of Materials Chemistry A

ROYAL SOCIETY OF CHEMISTRY

PAPER

View Article Online
View Journal | View Issue

Cite this: J. Mater. Chem. A, 2023, 11, 21203

Development of MOF-5-like ultra-microporous metal-squarate frameworks for efficient acetylene storage and separation†

Hai-Peng Li,[ab] Jia-Wen Wang[a] and Quan-Guo Zhai *[a]

Received 8th August 2023
Accepted 6th September 2023

DOI: 10.1039/d3ta04732f

rsc.li/materials-a

Although MOF-5 and its related family members are landmark metal–organic frameworks (MOFs), they have large specific surface area and high porosity, which have long been a subject regarding their instability. The introduction of new inorganic building blocks, in addition to classical $[Zn_4O(COO)_6]$, is a promising way to maintain the highly attractive architecture of MOF-5. Herein, a family of new MOF-5-like frameworks were synthesized by using squaric acid (SQ) and transition metal salts, namely, $\{(NH(CH_3)_2)_2[M_4X_4(SQ)_3]\}_n$ (SNNU-505-M, M = Zn, Co and Ni, X = F^- and OH^-). In this SNNU-505-M series of compounds, except for the μ_3-bridging atom of SNNU-505-Zn being an F^- ion, all the others are OH^-. Compared with MOF-5, SNNU-505-M exhibits good stability in organic solvent and aqueous solutions (pH = 3–13). Furthermore, benefiting from its ultra-micropore size and multiple polarity F^-/OH^- adsorption sites, SNNU-505-M shows high C_2H_2 adsorption capacity and excellent separation performance. In particular, SNNU-505-Zn exhibits the best C_2H_2/C_2H_4 (1 : 1) separation performance and its breakthrough interval time is 51 min g^{-1} at 298 K at a flow rate of 2 mL min^{-1}. The GCMC calculations further demonstrate that the excellent C_2H_2 uptake and C_2H_2/C_2H_4 separation performance of SNNU-505-Zn can be mainly attributed to the multiple C–H···F hydrogen bonds between the C_2H_2 molecules and MOF skeleton.

Introduction

Acetylene (C_2H_2) is a crucial chemical raw material mainly manufactured *via* the thermal cracking of hydrocarbons,[1] which usually coexists with some byproducts, such as ethylene (C_2H_4), carbon dioxide (CO_2) and methane (CH_4). To meet the needs of industrial applications, it is an urgent requirement to purify the C_2H_2 from C_2H_2/C_2H_4 and C_2H_2/CO_2 mixtures.[2–5] However, the molecular size and physicochemical properties of C_2H_2, C_2H_4 and CO_2 gas molecules are similar, which makes it a great challenge to separate them.[6] Currently, although solvent extraction, catalytic hydrogenation or cryogenic distillation methods are used to remove the C_2H_2 from C_2H_4 and separate CO_2 from C_2H_2, these purification technologies are energy intensive and environmentally unfriendly.[7] The drawbacks of these methods prompt the need to develop more energy efficient and environmentally friendly approaches for C_2H_2 capture and purification. Compared to the solvent extraction, catalytic hydrogenation and cryogenic distillation methods, by using porous materials, energy efficient and environmentally friendly adsorptive separation approaches have been developed and have attracted much attention.[8]

Among porous materials, metal–organic frameworks (MOFs), with their characteristic high surface area, high porosity, adjustable pore size and flexible framework structure, are relatively new types of porous materials that have shown great potential in gas adsorption and separation.[9] The concept of a MOF was first proposed by Yaghi in 1995.[10] Later, Yaghi and coworker reported a landmark MOF material, namely MOF-5.[11] In the MOF-5 framework, all the Zn^{2+} ions are four-coordinated, and the four Zn^{2+} ions are bridged by a μ_4-O atom to form a classical $Zn_4O(COO)_6$ metal cluster, which is further connected to six neighbors by six 1,4-dicarboxybenzenes to form a three-dimensional framework with a *pcu* topology. In 2005, using a variety of linear dicarboxylic ligands, Yaghi synthesized a series of isoreticular metal–organic frameworks (IRMOFs).[12] Although the specific surface area and pore size of these MOF-5-like structures can be regulated by using different dicarboxylate ligands, the frameworks of these MOF-5-like materials are unstable and they collapse rapidly in the presence of air and

[a]Institute of New Concept Sensors and Molecular Materials, Key Laboratory of Applied Surface and Colloid Chemistry, Ministry of Education, School of Chemistry& Chemical Engineering, Shaanxi Normal University, Xi'an, Shaanxi, 710062, China. E-mail: zhaiqg@snnu.edu.cn

[b]Ningxia Key Laboratory of Green Catalytic Materials and Technology, College of Chemistry and Chemical Engineering, Ningxia Normal University, Guyuan, 756000, China

† Electronic supplementary information (ESI) available: Experimental details, single crystal data, PXRD patterns, gas adsorption isotherms, IAST selectivity data, gas breakthrough curves, GCMC simulation results. CCDC 2269215 and 2269216. For ESI and crystallographic data in CIF or other electronic format see DOI: https://doi.org/10.1039/d3ta04732f

water vapor. In order to elevate the stability of such MOF-5-like frameworks, many scientists have focused on synthesizing densely arranged, highly connected, and complex structures, which are conducive to structural stability. However, in the field of gas adsorption and separation, in order to prepare MOF materials with simultaneous good stability and high porosity, researchers have to increase the packing density of MOF by reducing the size of the organic ligands, so as to improve the stability of the framework. Among them, squaric acid as an ideal small-sized organic ligand has attracted much attention. Notably, squaric acid-based MOFs have shown outstanding performance for gas adsorption and separation, with materials such as UTSA-280,[13] $[Co_3(C_4O_4)_2(OH)_2]\cdot 3H_2O$, and ZrSQU having been reported.[14–16] However, compared to other diptotic dicarboxylate ligands, such as oxalic acid and terephthalic acid, porous metal-squarate frameworks are very limited due to their strong acidity. Therefore, it is necessary to further expand the structure of such MOF materials, and screen out MOF materials that have a stable structure and excellent performance to achieve industrial applications.

Fortunately, in addition to regulating organic ligands, inorganic secondary building units can also be regulated during the synthesis of MOF materials.[17] Without changing the structural framework of these materials, the stability of MOF materials can be improved by increasing the bond number between metal ions and organic ligands through the regulation of inorganic secondary building units. For instance, Rosi and co-workers reported a series of MOF-5-like frameworks (MOF-1114).[18] Different from MOF-5, all the rare earth (RE) metals in the MOF-1114 structure are 10-coordinated, in which four rare earth metals are connected by four μ_3-OH bridging to form a $RE_4(\mu_3\text{-}OH)_4$ cuboxane type cluster, and the $RE_4(\mu_3\text{-}OH)_4$ cluster is further connected to its six neighbors by six 2-amino-terephthalic acid ligands to generate a 3D framework with *pcu* topology. The synthesis of MOF-1114 not only expands the types of metals used to prepare MOF-5-like framework, but also increases the coordination number of the metals, which is more conducive to the stability of the MOF framework. However, MOF-1114 has a relatively large pore size of 10 Å × 10 Å, which is not conducive to its application in the field of gas adsorption separation. In other words, in order to make MOF-5-like structures suitable for gas adsorption and separation, the metal types, framework stability, and pore sizes all need to be regulated.

Herein, by using squaric acid and 3d transition metal salts, a series of MOF-5-like ultramicroporous frameworks is reported with the molecular formula $\{(NH(CH_3)_2)_2[M_4X_4(SQ)_3]\}_n$ (SNNU-505-M, M = Zn, Co, Ni, X = F^-, OH^-). Interestingly, compared with the reported MOF-5-like frameworks, the synthesis of SNNU-505-M is improved in the following ways: (i) expanding the metal ion species. The metal ions in SNNU-505 can be Zn, Co, or Ni; (ii) the coordination number of the metal is increased and the stability of the framework is enhanced. The structure of SNNU-505-Zn remained stable before and after solvent exchange, before and after gas adsorption and separation performance tests, and after soaking in pH = 3–13 solution for 24 h; (iii) the pore size is decreased. The aperture size in SNNU-505-M is only 4.5 Å, which is conducive to SNNU-505-M used to gas adsorption and separation; (iv) introducing abundant adsorption sites. There are a large number of bridging F^- or OH^- in the SNNU-505-M framework. Furthermore, the gas adsorption results show that SNNU-505-M exhibits excellent performance in C_2H_2 uptake, especially SNNU-505-Zn, the C_2H_2 uptake of which exceeds those of many reported MOF materials at 298 K and 0.25 atm. In addition, SNNU-505-Zn also exhibits the best C_2H_2/C_2H_4 separation performance due to the presence of multiple strong hydrogen bond receptor F^- ions in the SNNU-505-Zn channels. Grand Canonical Monte Carlo (GCMC) simulations were further used to explain the strong interaction between SNNU-505-Zn and gas molecules.

Experimental section

Materials and measurements

All chemical reagents were purchased from commercial suppliers. Powder X-ray diffraction (PXRD) data were collected on a Rigaku MiniFlex-600 (40 kV, 15 mA) diffractometer. Thermogravimetric analysis (TGA) curves were measured on a NETZSCH STA 449C thermal analyzer under a N_2 atmosphere at a heating rate of 2 °C min^{-1}. The single-crystal X-ray diffraction data of SNNU-505-Co were collected on a Bruker Smart APEX II CCD area diffractometer equipped with a Cu Kα radiation source (λ = 1.54184 Å). The single-crystal data of SNNU-505-Zn were collected on a Rigaku XtaLAB mini II CCD area diffractometer equipped with a Mo Kα radiation source (λ = 0.71073 Å). Structure refinements were carried out using SHELXTL.[19,20] The SQUEEZE program of the PLATON software package was used to remove the disordered solvent molecules.[21] The energy dispersive spectroscopy (EDS) data were collected on SNNU-505-Zn by using a Quanta 200 spectrometer (FEI Co. Ltd, USA).

Gas adsorption measurements

The gas adsorption isotherms of N_2 at 77 K and $C_2H_2/C_2H_4/CO_2$ at 273/298 K were collected on a Micromeritics 3-Flex surface-area and pore-size analyzer. Before gas adsorption isotherm measurements were carried out, the fresh MOF sample (100 mg) was soaked in acetone or methanol for four days; during this period, MOF samples were exchanged with fresh acetone or methanol solvent at least three times a day, then the samples were heated at 80 °C and 120 °C for 6 h under high vacuum, respectively.

Breakthrough curve measurements

The activated samples of SNNU-505-Zn (1.2 g) or SNNU-505-Co (1.2 g) were packed into stainless steel columns. Then, He gas with a total flow of 30 mL min^{-1} was swept into the columns to remove impurities. When the concentration of the impurity gas was below 10^{-8}, the breakthrough curve was collected on the Hiden HPR-20 R&D mass spectrometer.

GCMC simulations

The sorption module of the Material Studio Materials Studio 8.0 package was used to simulate the process of gas adsorption in SNNU-505-Zn.[22] The structure of SNNU-505-Zn was regarded as rigid, and all the gas molecules were optimized. A $2 \times 2 \times 2$ unit cell was used in all relevant simulations, and the cut-off radius was set to 18.5 Å. The max equilibration and production steps were 1×10^7. The universal force (UFF) was used to determine the strength of gas-framework and gas–gas interactions.

Synthesis of $\{(NH(CH_3)_2)_2[Zn_4F_4(SQ)_3]\}_n$ (SNNU-505-Zn-a)

Method A. In a 20 mL screw-capped vial, 0.059 g of $Zn(SiF_6)_2 \cdot 6H_2O$, 0.030 g of squaric acid (SQ) and 0.018 g of pyrazine were dissolved in a solvent mixture of DMF/MeOH/H_2O (3/1/0.5, v/v/v). The mixture was stirred for 30 min, then the screw-capped vial was heated to 120 °C for 2 days. Finally, the red cubic crystals obtained were washed with DMF and MeOH (Fig. S2a†).

Method B. Method B is the same as method A except that the metal salt was changed from $Zn(SiF_6)_2 \cdot 6H_2O$ to $Zn(BF_4)_2 \cdot 4H_2O$. Finally, the mixture solvent was heated to 120 °C for 3 days, after which light-orange cubic crystals were obtained. The crystals were washed with DMF and MeOH.

Synthesis of $\{(NH(CH_3)_2)_2[Co_4(OH)_4(SQ)_3]\}_n$ (SNNU-505-Co)

Method A. In a 20 mL screw-capped vial, 0.052 g of $Co(OAc)_2 \cdot 4H_2O$, 0.025 g of SQ and 0.015 g of isonicotinic acid were dissolved in a solvent mixture of DMF/H_2O (3/0.5, v/v), the mixture was stirred for 2 h, then the screw-capped vial was heated to 135 °C for 3 days. Finally, the obtained red polyhedral block crystals were washed with DMF and MeOH (Fig. S2b†).

Method B. In a 20 mL screw-capped vial, 0.059 g of $CoSO_4 \cdot 7H_2O$, 0.025 g of SQ and 0.018 g of pyrazine were dissolved in a solvent mixture of DMF/MeOH/H_2O (3/1/0.5, v/v/v). The mixture was stirred for 2 h, then the screw-capped vial was heated to 120 °C for 3 days. The obtained red cubic crystals were filtered and washed with DMF and MeOH.

Synthesis of $\{(NH(CH_3)_2)_2[Ni_4(OH)_4(SQ)_3]\}_n$ (SNNU-505-Ni)

In a 20 mL screw-capped vial, 0.075 g of $NiCl_2 \cdot 6H_2O$ and 0.025 g of SQ were dissolved in a solvent mixture of DMF/MeOH/DMSO (3/1/1, v/v). Then, three drops of HBF_4 (fluoroboric acid, 40% in water) were added to the solution and the mixture was stirred for 2 h, before heating the screw-capped vial to 120 °C for 7 days. The obtained green powder sample was filtered and washed with DMF and MeOH.

Results and discussion

Crystal structures of SNNU-505-M

The single-crystal X-ray diffraction data indicate that the SNNU-505-M samples are isoreticular, and all the MOFs crystallized in the cubic $Fm\bar{3}m$ space group (Tables S1–S3†). As shown in Fig. 1, the asymmetric unit of SNNU-505-M comprises one metal ion, a quarter of one squaric acid linker and one μ_3-OH^-/F^- ion. Four metal ions are connected by four μ_3-OH^-/F^- ions to form a cubane M_4X_4 (M = Zn, Co, Ni; X = OH^-/F^-) polymetallic cluster (Fig. 1h). Each cubane M_4X_4 cluster is co-planar connected to the six surrounding M_4X_4 clusters by a six squaric acid linker to generate a three-dimensional framework with *pcu* type topology (Fig. 1i and S1†). In the SNNU-505-M series of compounds, except for the μ_3 bridging atom of SNNU-505-Zn being a F^- ion, all the others are OH^-. The EDS results indicate that F anions exist in the framework of SNNU-505-Zn (Fig. S3†). Detailed structure analysis of SNNU-505-M shows that SNNU-505 and IRMOF have the same topological structure. In the IRMOF crystal structure,[11,12] the difference is that four Zn^{2+} ions are bridged by a μ_4-O atoms to form a classical tetrahedral $[Zn_4O(COO)_6]$ cluster (Fig. 1b), and all the Zn^{2+} ions are four-connected. Each tetrahedral metal cluster co-edge connects the six surrounding tetrahedral metal clusters *via* six BDC ligands to form an IRMOF structure with *pcu* topology (Fig. 1c). However, due to the Zn^{2+} ions in the IRMOF framework being 4-connected, this greatly limits the extending of the structure and significant decreases the stability of the IRMOF. This is because the usual coordination number of most transition metal ions and main group metal ions is six, and only a few Co^{2+} and Ni^{2+} metal ions exhibit four-coordination, such as the ZIF series of compounds. At the same time, the stability of IRMOF is poor because Zn^{2+} ions are soft bases and carboxylic ligands are hard acids, and the Zn–O coordination bond is easily broken by the attack of solvent molecules. Besides, Rosi and co-workers reported a series of $RE_4(\mu_3\text{-}OH)_4(COO)_6^{2+}$ cluster-based MOF materials (MOF-1114) with *pcu* type topology (Fig. 1d–f).[18] The coordination number of MOF-1114 is higher than that of IRMOF, and the metal ion range was expanded to include rare earth (RE^{3+}) metals. Compared with IRMOF and MOF-1114, in our study, by further shortening the ligand, a series of ultramicroporous MOF materials (SNNU-505-M) with *pcu* topology were synthesized using squaric acid as a ligand and transition metal ions. Fortunately, in SNNU-505-M, all the metals are six-coordinate, which greatly improves the compatibility of metals and has great expansibility. The SNNU-505 structure is more stable than the IRMOF. In addition, the pore size of SNNU-505 can be reduced to 4.5 Å by shortening the length of the dicarboxylic acid ligand (Fig. 1i), and there are a large number of OH^- or F^- ions in the channel, which is expected to achieve excellent C_2H_2 adsorption and separation performance by strong C–H···X hydrogen bonding.

The stability and purity of SNNU-505-M were proved by collecting the powder X-ray diffraction data at room temperature. As shown in Fig. S4,† SNNU-505-Zn is stable in different pH solutions, and in all the test processes, SNNU-505-M still retains high crystallinity. Furthermore, the thermogravimetric curves of SNNU-505-M indicated that all the MOF frameworks are stable up to 250 °C. The TG curves of the SNNU-505-M series of compounds show two obvious weight loss phenomena, and the first step weight loss occurs before 100 °C, which is due to the removal of solvent molecules. An obvious plateau is observed at 100–250 °C, which is the stable period of the MOF framework. The second weight loss occurs

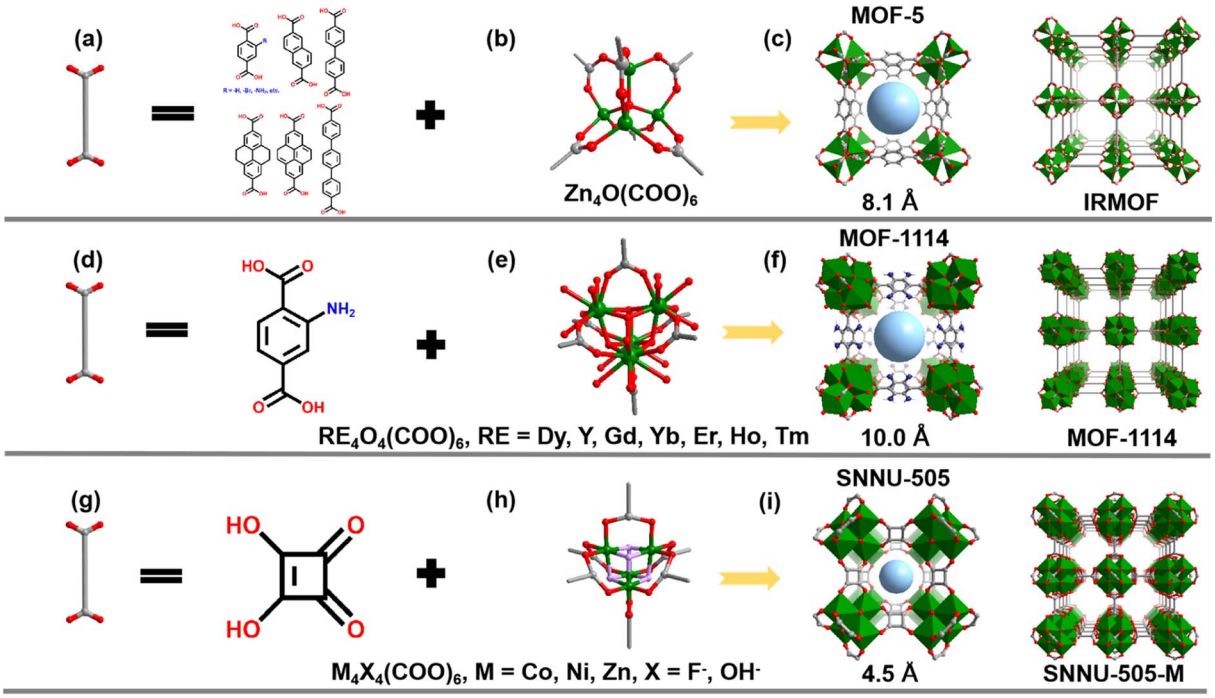

Fig. 1 Crystal structures of the MOF-5-like materials: (a–c) IRMOF; (d–f) MOF-1114; (g–i) SNNU-505-M.

at 250–350 °C; the weight loss in this process can be attributed to the decomposition of ligands. Finally, the MOF framework completely collapses (Fig. S5†).

Gas adsorption properties of SNNU-505-M

The PLATON calculation results indicated that the guest accessible volume for SNNU-505-Zn is 4071.8 $Å^3$, and the value for SNNU-505-Co is 4071.8 $Å^3$, values which occupy approximately 58.7% and 59.3% of the entire crystal volume. In addition, the N_2 adsorption isotherms for SNNU-505-M were measured at 77 K. As illustrated in Fig. S6a,† the results show that SNNU-505-M can uptake 119.9 $cm^3\ g^{-1}$ (SNNU-505-Zn), 109.8 $cm^3\ g^{-1}$ (SNNU-505-Co), and 135.0 $cm^3\ g^{-1}$ (SNNU-505-Ni) of N_2 at 1 atm, respectively. The corresponding BET surface areas are 493.5 $m^2\ g^{-1}$ (SNNU-505-Zn), 417 $m^2\ g^{-1}$ (SNNU-505-Co), and 469.9 $m^2\ g^{-1}$ (SNNU-505-Ni). Furthermore, the calculation results based on the Horvath–Kawazoe model show that the pore size is mainly distributed between 5.5 Å and 6.4 Å, which matches the window size (4.7 Å) and cage size (6.0 Å) of SNNU-505-M. In addition, we also recorded the CO_2 adsorption isotherm for SNNU-505-M at 195 K, which indicates that SNNU-505-Zn, SNNU-505-Co and SNNU-505-Ni can uptake 94 $cm^3\ g^{-1}$, 85 $cm^3\ g^{-1}$ and 89 $cm^3\ g^{-1}$ of CO_2 at 195 K and 1 atm, with corresponding BET surface areas of 276.8 $m^2\ g^{-1}$, 180 $m^2\ g^{-1}$ and 186 $m^2\ g^{-1}$, respectively, and the pore sizes are primarily distributed around 4.8 Å (Fig. 2a). Notably, the BET surface area values obtained from the adsorption curves for N_2 at 77 K and CO_2 at 195 K are different due to the quadrupole moments of N_2 and CO_2 being different, which leads to different adsorption behavior, diffusion rate and arrangement mode in their channels.

The suitable pore size and multiple polarity adsorption sites in SNNU-505-M encouraged the further comparison of the gas adsorption performance to explain the effect of polarity adsorption site on gas adsorption and separation. First, at 273/298 K and 1 atm, the C_2H_2 adsorption isotherms for SNNU-505-M were measured. As shown in Fig. 2b and S6b,† the adsorption isotherms of C_2H_2 exhibit a type-I isotherm, and the adsorption capacity of the MOF framework basically reaches saturation when the pressure is around 200 mmHg. In particular, SNNU-505-Zn can uptake 60 $cm^3\ g^{-1}$ of C_2H_2 at 298 K and 0.25 atm (190 mmHg), as shown in Fig. 3f, a higher capacity than many MOF absorbents, such as SNNU-150-Al,[23] HIAM-210,[24] and NUM-14.[25] When the pressure is 1 atm, SNNU-505-Zn can uptake 67.5 $cm^3\ g^{-1}$ of C_2H_2 at 298 K. The relative value for SNNU-505-Co is 52.7 $cm^3\ g^{-1}$ and that for SNNU-505-Ni is 63.4 $cm^3\ g^{-1}$. With a reduction in temperature, the adsorption performance of SNNU-505-M increases. At 273 K and 1 atm, the C_2H_2 capacity is 73.5 $cm^3\ g^{-1}$ for SNNU-505-Zn, 64.2 $cm^3\ g^{-1}$ for SNNU-505-Co and 75.4 $cm^3\ g^{-1}$ for SNNU-505-Ni. As illustrated in Fig. 2b–d and S6,† compared with the acetylene adsorption isotherm, the slope of the C_2H_4 and CO_2 adsorption isotherm is significantly lower. This phenomenon indicates that the selectivity of SNNU-505-M to C_2H_2 is stronger than that of C_2H_4 and CO_2. At 273/298 K and 1 atm, the uptakes of C_2H_4 and CO_2 are 59/46.67 $cm^3\ g^{-1}$ and 81/58.8 $cm^3\ g^{-1}$ for SNNU-505-Zn, the corresponding values of which for SNNU-505-Co are 41.3/30.9 and 43.7/30.3 $cm^3\ g^{-1}$, and for SNNU-505-Ni are 51.8/40.81 and 67.84/47.8 $cm^3\ g^{-1}$. It can be seen that although the adsorption capacity of these compounds is not high, the adsorption properties are regulated systematically through the introduction of different

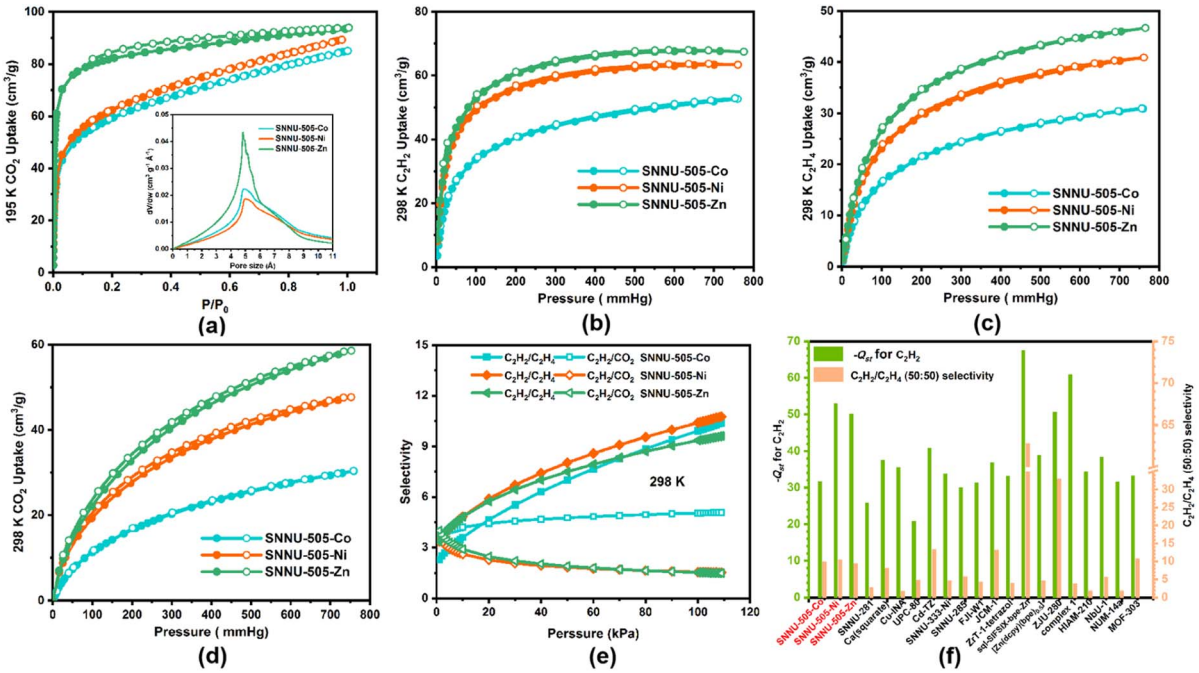

Fig. 2 (a) The CO_2 adsorption and desorption isotherms at 195 K, (b) the C_2H_2, (c) C_2H_4 and (d) CO_2 uptake isotherms at 298 K, (e) a IAST selectivity summary of C_2H_2/C_2H_4 (50 : 50) and C_2H_2/CO_2 (50 : 50) at 298 K, and (f) the selectivity of C_2H_2/C_2H_4 (50 : 50) at 1 atm *vs.* the C_2H_2 $-Q_{st}$ at zero loading for SNNU-505-M and some published MOF materials.

polar adsorption sites. In particular, the SNNU-505-Zn with polar F^- ion sites exhibits excellent acetylene adsorption properties under low pressure.

To further understand the effect of polar adsorption sites on gas adsorption and separation performance, the virial model was used to calculate the isosteric heat of adsorption ($-Q_{st}$). As

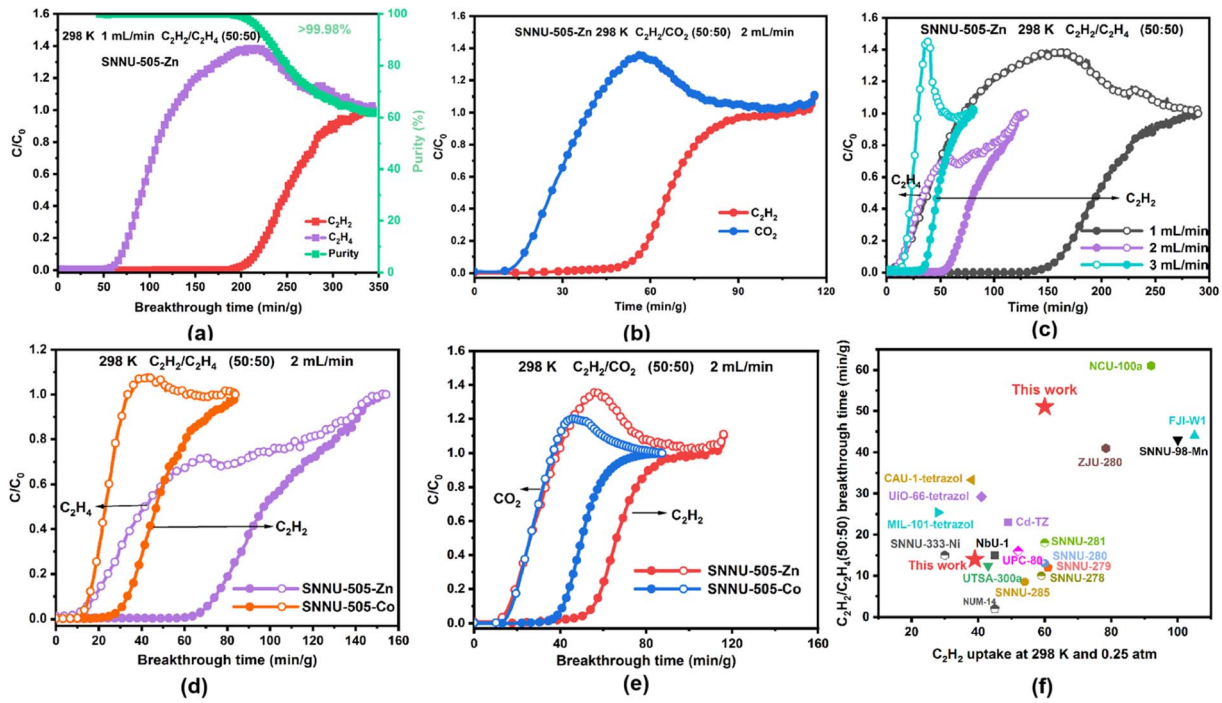

Fig. 3 The breakthrough curve for SNNU-505-Zn, (a) the C_2H_2/C_2H_4 (50 : 50) breakthrough curve at 298 K and the total flow of 1 mL min^{-1}, (b) the C_2H_2/CO_2 (50 : 50) breakthrough curve at 298 K and the total flow of 2 mL min^{-1}, (c) the C_2H_2/C_2H_4 (50 : 50) breakthrough curve at 298 K and the different total flows, a comparison of the breakthrough results of (d) C_2H_2/C_2H_4 and (e) C_2H_2/CO_2 for SNNU-505-M, and (f) the comparison results between SNNU-505-M and the MOF absorbents with excellent performance towards C_2H_2/C_2H_4 at 298 K.

shown in Fig. 2f and S7–S10,† the C_2H_2 isosteric heat of SNNU-505-Zn is 50.7 kJ mol^{-1} at zero coverage, which is almost equal to that of SNNU-505-Ni (52.9 kJ mol^{-1}) and higher than that of SNNU-505-Co (31.7 kJ mol^{-1}). Compared with the $-Q_{st}$ value of C_2H_2, the C_2H_4 and CO_2 isosteric heats are significantly decreased. The $-Q_{st}$ values of C_2H_4 and CO_2 are 34.9 kJ mol^{-1} and 41.7 kJ mol^{-1} for SNNU-505-Zn, respectively. The corresponding values are 31.7 kJ mol^{-1} and 38.8 kJ mol^{-1} for SNNU-505-Co, and 33.0 kJ mol^{-1} and 41.4 kJ mol^{-1} for SNNU-505-Ni. Remarkably, the $-Q_{st}$ values of C_2H_2 for SNNU-505-Zn and SNNU-505-Ni are equal to those of many famous MOF absorbents, such as SIFSIX-2-Cu-i (52.7 kJ mol^{-1}),[26] ZJU-280 (50.6 kJ mol^{-1}) and NbOFFIVE-dp-Cu (52.7 kJ mol^{-1}),[27,28] and higher than those of SNNU-12 (21.3 kJ mol^{-1}),[29] NTU-60 (26.9 kJ mol^{-1}) and SIFSIX-2-Cu (26.3 kJ mol^{-1}) (Fig. 2f).[26,30] In addition, the calculation results of the $-Q_{st}$ values indicated that SNNU-505-M can effectively separate C_2H_2/C_2H_4 and C_2H_2/CO_2 mixtures.

C_2H_2/C_2H_4 and C_2H_2/CO_2 selectivity

Considering SNNU-505-M with a suitable pore size and as a multiple strong hydrogen bond receptor, the ideal adsorption solution theory (IAST) was used to calculate the selectivity of SNNU-505-M for both C_2H_2/C_2H_4 (50 : 50) and C_2H_2/CO_2 (50 : 50) at 273/298 K. As shown in Fig. 2e, f and S11–S14,† the equimolar binary mixture C_2H_2/C_2H_4 and C_2H_2/CO_2 IAST selectivities are in the range of 3.4–9.4 and 4.0–1.5 for SNNU-505-Zn at 298 K, respectively, where the corresponding IAST selectivities are 2.3–10.0 and 3.6–5.1 for SNNU-505-Co, and 3.4–10.4 and 3.7–1.5 for SNNU-505-Ni. Clearly, SNNU-505-M exhibits excellent IAST selectivity for C_2H_2/C_2H_4 and C_2H_2/CO_2 mixtures at 298 K. In particular, the C_2H_2/CO_2 IAST selectivity of SNNU-505-Zn is equal to those of many promising adsorbents, such as FJU-90 (4.3),[31] ZrT-1-tetrazol (4.05),[32] JNU-1 (3.6) and SNNU-27-Fe (3.6),[33,8c] *etc.* In addition, as shown in Fig. 2f, the C_2H_2/C_2H_4 (50 : 50) selectivity is higher than those of many MOF materials. When the temperature decreases to 273 K, the C_2H_2/C_2H_4 and C_2H_2/CO_2 IAST selectivities are 1.98–5.17 and 2.6–1.4 for SNNU-505-Zn, 2.0–10.0 and 3.2–3.7 for SNNU-505-Co, and 2.8–9.8 and 3.3–2.2 for SNNU-505-Ni. The high C_2H_2 uptake at low pressure, high C_2H_2 $-Q_{st}$ and prominent IAST selectivity indicate that SNNU-505-M can potentially separate C_2H_2/C_2H_4 and C_2H_2/CO_2 mixtures.

Breakthrough experiments for SNNU-505-M

To evaluate the practical C_2H_2/C_2H_4 and C_2H_2/CO_2 separation performance of SNNU-505-M, the breakthrough experiment data at 273/283/298 K and 1 atm for SNNU-505-M were collected using a home-made breakthrough instrument (Fig. S15†). As shown in Fig. 3 and S16–S21,† C_2H_4 and CO_2 were first eluted in the adsorbent bed, and the C_2H_2 was retained in the adsorbent bed, successfully proving the excellent separation performance of SNNU-505-M toward the C_2H_2/C_2H_4 and C_2H_2/CO_2 equimolar binary mixtures. For the C_2H_2/C_2H_4 (50 : 50) mixture with a total flow of 2 mL min^{-1}, C_2H_4 was absorbed in the fixed-bed column packed with SNNU-505-Zn (1.2 g) samples for around 40 min g^{-1} and then flowed out of the fixed-bed, and C_2H_4 was eluted in the bed with high purity (>99.98%). After 75 min g^{-1} (273 K) and 51 min g^{-1} (298 K), C_2H_2 broke out. The breakthrough times of SNNU-505-Zn are 75 min g^{-1} (273 K) and 51 min g^{-1} (298 K) at a total flow of 2 mL min^{-1}, respectively, which indicate that SNNU-505-Zn can uptake 5.1 mmol g^{-1} and 4.0 mmol g^{-1} of C_2H_2 at 273 K and 298 K (Fig. S17a† and 3a). The breakthrough data did not show any significant changes after three cycles (Fig. S18†). Furthermore, breakthrough experiments were also conducted at different temperature and flows, the results of which indicated that SNNU-505-Zn also has the capacity to separate a C_2H_2/C_2H_4 (1 : 99) binary mixture. In addition, it is worth noting that the C_2H_2/C_2H_4 breakthrough time of SNNU-505-Zn reached 125 min g^{-1} at 298 K and a total flow of 1 mL min^{-1}, a performance that is better than those of many MOF adsorbents (Fig. 3f).[34–43] For the C_2H_2/CO_2 (50 : 50) mixture with a total flow of 2 mL min^{-1}, the breakthrough time of SNNU-505-Zn reached 48 min g^{-1} (273 K) and 33 min g^{-1} (298 K). Therefore, all the breakthrough results present that SNNU-505-Zn can efficiently separate C_2H_2/C_2H_4 and C_2H_2/CO_2 mixtures.

In addition, in order to investigate the influence of F^-/OH^- polar adsorption sites modified in the channel of SNNU-505-M on the gas adsorption and separation performance, the equimolar C_2H_2/C_2H_4 and C_2H_2/CO_2 binary mixture breakthrough curves of SNNU-505-Co (1.2 g) were also collected. As shown in Fig. 3d–e and S21,† due to the interaction between polar OH^- and gas molecules being weaker than that of F^- ions, the breakthrough time and uptake of SNNU-505-Co are poorer than those of SNNU-505-Zn. At 298 K and a total flow of 2 mL min^{-1}, the C_2H_2/C_2H_4 (50 : 50) and C_2H_2/CO_2 (50 : 50) breakthrough times of SNNU-505-Co are 14 min g^{-1} and 20 min g^{-1}, respectively. When the temperature is 273 K, the breakthrough times of SNNU-505-Co are 25 min g^{-1} (C_2H_2/C_2H_4, 50 : 50) and 20 min g^{-1} (C_2H_2/CO_2, 50 : 50). In short, the suitable pore size and the polar adsorption sites in the pore regulated the separation performance of SNNU-505-M. Moreover, because the electronegativity of F is greater than that of O, the separation performance of SNNU-505-Zn is much higher than that of the other compounds.

GCMC simulations

In order to further understand the interaction between gas molecules and the MOF absorbent, GCMC calculations were used to simulate the gas adsorption and separation process of SNNU-505-Zn. As depicted in Fig. 4 and S22,† the GCMC calculation results show that the interaction between the C_2H_2 molecules and SNNU-505-Zn framework can adopt the following three forms: (i) the C_2H_2 molecules are primarily distributed around the Zn_4F_4 metal clusters, and bind to F^- polar adsorption sites through multiple strong hydrogen bonds (C–H$\cdots$F) with bond lengths in the range of 2.4–3.8 Å. (ii) A small portion of C_2H_2 gas is distributed around the squaric acid, which binds *via* intense $\pi\cdots$H–C interactions with a bond length in the range of 3.3–3.9 Å. (iii) A small portion of the C_2H_2 molecules are distributed around the squaric acid, which bind

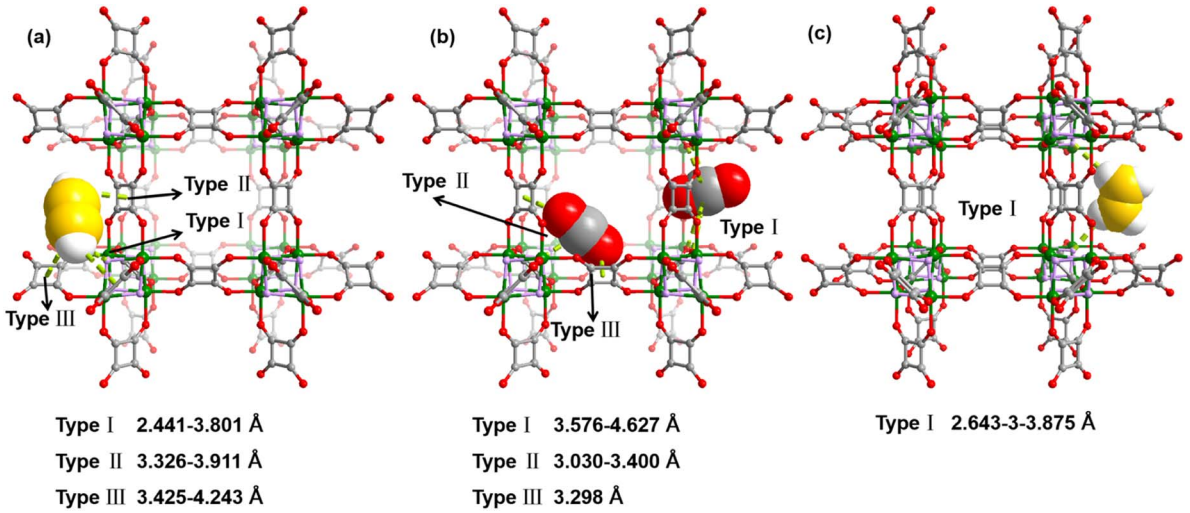

Fig. 4 The distributions of (a) C_2H_2, (b) CO_2 and (c) C_2H_4 in SNNU-505-Zn.

via intense π···π interactions with a bond length in the range of 3.4–4.2 Å. Compared to C_2H_2 molecules, the interaction between CO_2 molecules and the SNNU-505-Zn framework weakens, where the interaction is of the following three types: the CO_2 is distributed in the one side of the channel of SNNU-505-Zn, where there are multiple C–O···C_{CO_2} interactions with a bond distance in the range of 3.6–4.6 Å (Fig. S20c†). There are also strong F···C_{CO_2} and π···O–C interactions with a bond length in the range of 3.0–3.4 Å. For C_2H_4, the main interaction is a C–H···F hydrogen bond interaction with a bond distance in the range of 2.6–3.9 Å. The GCMC calculation results significantly explain the adsorption performance of SNNU-505-Zn (C_2H_2 > CO_2 > C_2H_4) and match the breakthrough experiment and $-Q_{st}$ calculation results, which further proves that SNNU-505-Zn exhibits excellent separation performance for binary C_2H_2/CO_2 and C_2H_2/C_2H_4 mixtures.

Conclusions

In summary, by using squaric acid (SQ) and transition metal salts, a series of MOF-5-like frameworks were successfully obtained. In addition, ascribed to the ultramicroporous characteristics and multiple polar adsorption sites modification of SNNU-505-M, all the MOF materials show selective adsorption of C_2H_2 and have excellent separation performance toward C_2H_2/C_2H_4 and C_2H_2/CO_2 binary mixture. In particular, due to the polar F^- ions in the SNNU-505-Zn framework forming strong C–H···F hydrogen bonds with C_2H_2 molecules, SNNU-505-Zn exhibits the best C_2H_2/C_2H_4 separation performance. The synthesis of these series of compounds expands the types of metals that can be used in the MOF-5 framework, and a new F-MOF material was also developed, which serves as a reference for the development of MOF materials in the adsorption and separation field in the future.

Conflicts of interest

There are no conflicts to declare.

Acknowledgements

This work was financially supported by the National Natural Science Foundation of China (22071140), the Natural Science Foundation of Shaanxi Province (2021JLM-20), the Fundamental Research Funds for the Central Universities (GK202307009), and the Youth Innovation Team of Shaanxi Universities (2023).

Notes and references

1 P. Pässler; W. Hefner; K. Buckl, H. Meinass, A. Meiswinkel, H.-J. Wernicke, G. Ebersberg, R. Müller, J. Bässler, H. Behringer, and D. Mayer, *Ullmann's Encyclopedia of Industrial Chemistry*, Wiley-VCH, Weinheim, Germany, 2000.
2 J. Shen, X. He, T. Ke, R. Krishna, J. M. van Baten, R. Chen, Z. Bao, H. Xing, M. Dincă, Z. Zhang, Q. Yang and Q. Ren, *Nat. Commun.*, 2020, **11**, 6259.
3 T. Ke, Q. Wang, J. Shen, J. Zhou, Z. Bao, Q. Yang and Q. Ren, *Angew. Chem., Int. Ed.*, 2020, **59**, 12725–12730.
4 Q. Dong, X. Zhang, S. Liu, R.-B. Lin, Y. Guo, Y. Ma, A. Yonezu, R. Krishna, G. Liu, J. Duan, R. Matsuda, W. Jin and B. Chen, *Angew. Chem., Int. Ed.*, 2020, **59**, 22756–22762.
5 Y.-L. Peng, T. Pham, P. Li, T. Wang, Y. Chen, K.-J. Chen, K. A. Forrest, B. Space, P. Cheng, M. J. Zaworotko and Z. Zhang, *Angew. Chem., Int. Ed.*, 2018, **57**, 10971–10975.
6 (*a*) K.-J. Chen, H. S. Scott, D. G. Madden, T. Pham, A. Kumar, A. Bajpai, M. Lusi, K. A. Forrest, B. Space, J. J. Perry IV and M. Zaworotko, *J. Chem.*, 2016, **1**, 753–765; (*b*) K.-J. Chen, D. G. Madden, S. Mukherjee, T. Pham, K. A. Forrest, A. Kumar, B. Space, J. Kong, Q.-Y. Zhang and M. J. Zaworotko, *Science*, 2019, **366**, 241–246; (*c*) J.-W. Wang, S.-C. Fan, H.-P. Li, X. Bu, Y.-Y. Xue and Q.-G. Zhai, *Angew. Chem., Int. Ed.*, 2023, **62**, e202217839.
7 (*a*) E. D. Bloch, W. L. Queen, R. Krishna, J. M. Zadrozny, C. M. Brown and J. R. Long, *Science*, 2012, **335**, 1606–1610; (*b*) Z. J. Zhang, Z.-Z. Yao, S. Xiang and B. Chen, *Energy*

Environ. Sci., 2014, **7**, 2868–2899; (*c*) H.-P. Li, Z.-D. Dou, Y. Xiao, G.-J. Fan, D.-C. Pan, M.-C. Hu and Q.-G. Zhai, *Nanoscale*, 2022, **14**, 18200–18208.

8 (*a*) X. Zhao, Y. X. Wang, D.-S. Li, X. H. Bu and P. Y. Feng, *Adv. Mater.*, 2018, **30**, 1705189–1705222; (*b*) L. F. Yang, S. H. Qian, X. B. Wang, X. L. Cui, B. L. Chen and H. B. Xing, *Chem. Soc. Rev.*, 2020, **49**, 5359–5406; (*c*) Y.-Y. Xue, X.-Y. Bai, J. Zhang, Y. Wang, S.-N. Li, Y.-C. Jiang, M.-C. Hu and Q.-G. Zhai, *Angew. Chem., Int. Ed.*, 2021, **60**, 10122–10128.

9 (*a*) Z. Di, X. Zheng, Y. Qi, H. Yuan and C.-P. Li, *Chin. J. Struct. Chem.*, 2022, **41**, 2211031–2211044; (*b*) L. Li, L. Guo, Z. Zhang, Q. Yang, Y. Yang, Z. Bao, Q. Ren and J. Li, *J. Am. Chem. Soc.*, 2019, **141**, 9358–9364; (*c*) L. F. Yang, S. H. Qian, X. B. Wang, X. L. Cui, B. L. Chen and H. B. Xing, *Chem. Soc. Rev.*, 2020, **49**, 5359–5406.

10 O. M. Yaghi, G. Li and H. Li, *Nature*, 1995, **378**, 703–706.

11 H. Li, M. Eddaoudi, M. O'Keeffe and O. M. Yaghi, *Nature*, 1999, **402**, 276.

12 J. L. C. Rowsell, E. C. Spencer, J. Eckert, J. A. K. Howard and O. M. Yaghi, *Science*, 2005, **309**, 1350–1354.

13 R.-B. Lin, L. Li, H.-L. Zhou, H. Wu, C. He, S. Li, R. Krishna, J. Li, W. Zhou and B. Chen, *Nat. Mater.*, 2018, **17**, 1128–1133.

14 L. Li, L. Guo, Z. Zhang, Q. Yang, Y. Yang, Z. Bao, Q. Ren and J. Li, *J. Am. Chem. Soc.*, 2019, **141**, 9358–9364.

15 B. Bueken, H. Reinsch, N. Reimer, I. Stassen, F. Vermoortele, R. Ameloot, N. Stock, C. E. A. Kirschhocka and D. D. Vos, *Chem. Commun.*, 2014, **50**, 10055–10058.

16 S. Kandambeth, V. S. Kale, D. Fan, J. A. Bau, P. M. Bhatt, S. Zhou, A. Shkurenko, M. Rueping, G. Maurin, O. Shekhah and M. Eddaoudi, *Adv. Energy Mater.*, 2023, **13**, 2202964.

17 (*a*) D. J. Tranchemontagne, J. L. Mendoza-Cortés, M. O'Keeffe and O. M. Yaghi, *Chem. Soc. Rev.*, 2009, **38**, 1257–1283; (*b*) W. Lu, Z. Wei, Z.-Y. Gu, T.-F. Liu, J. Park, J. Park, J. Tian, M. Zhang, Q. Zhang, T. Gentle III, M. Bosch and H.-C. Zhou, *Chem. Soc. Rev.*, 2014, **43**, 5561–5593; (*c*) W. Fan, S. Yuan, W. Wang, L. Feng, X. Liu, X. Zhang, X. Wang, Z. Kang, F. Dai, D. Yuan, D. Sun and H.-C. Zhou, *J. Am. Chem. Soc.*, 2020, **142**, 8728–8737.

18 T.-Y. Luo, C. Liu, S. V. Eliseeva, P. F. Muldoon, S. Petoud and N. L. Rosi, *J. Am. Chem. Soc.*, 2017, **139**, 9333–9340.

19 G. M. Sheldrick, *SHELXS-97*, University of Göttingen, Gottingen, Germany, 1997.

20 G. M. Sheldrick, *SHELXS-97, Program for the Crystal Structure Refinement*, University of Göttingen, Gottingen, Germany, 1997.

21 (*a*) A. L. Spek, Single-Crystal Structure Validation with the Program PLATON, *J. Appl. Crystallogr.*, 2003, **36**, 7–13; (*b*) O. V. Dolomanov, L. J. Bourhis, R. J. Gildea, J. A. K. Howard and H. Puschmann, *J. Appl. Crystallogr.*, 2009, **42**, 339–341.

22 A. K. Rappe and W. A. Goddard, *J. Phys. Chem.*, 1991, **95**, 3358–3363.

23 H.-J. Lv, J.-W. Zhang, Y.-C. Jiang, S.-N. Li, M.-C. Hu and Q.-G. Zhai, *Inorg. Chem.*, 2022, **61**, 3553–3562.

24 J. Liu, H. Wang and J. Li, *Chem. Sci.*, 2023, **14**, 5912–5917.

25 Q. Zhang, G.-N. Han, X. Lian, S.-Q. Yang and T.-L. Hu, *Molecules*, 2022, **27**, 5929.

26 X. Cui, K. Chen, H. Xing, Q. Yang, R. Krishna, Z. Bao, H. Wu, W. Zhou, X. Dong, Y. Han, B. Li, Q. Ren, M. J. Zaworotko and B. Chen, *Science*, 2016, **353**, 141–144.

27 (*a*) Q.-L. Qian, X.-W. Gu, J. Pei, H.-M. Wen, H. Wu, B. Li and G. Qian, *J. Mater. Chem. A*, 2021, **9**, 9248–9255; (*b*) L. Li, R.-B. Lin, R. Krishna, X. Wang, B. Li, H. Wu, J. Li, W. Zhou and B. Chen, *J. Mater. Chem. A*, 2017, **5**, 18984–18988.

28 J. Wang, Y. Zhang, Y. Su, X. Liu, P. Zhang, R.-B. Lin, S. Chen, Q. Deng, Z. Zeng, S. Deng and B. Chen, *Nat. Commun.*, 2022, **13**, 200.

29 J. W. Zhang, M. C. Hu, S. N. Li, Y. C. Jiang and Q.-G. Zhai, *Cryst. Growth Des.*, 2016, **16**, 6430–6435.

30 H. Wang, Y. Duan, Y. Wang, Y. Huang, K. Ge, S. Wang, B. Zheng, Z. Wang, J. Bai and J. Duan, *ACS Appl. Mater. Interfaces*, 2022, **14**, 13550–13559.

31 Y. Ye, Z. Ma, R.-B. Lin, R. Krishna, W. Zhou, Q. Lin, Z. Zhang, S. Xiang and B. Chen, *J. Am. Chem. Soc.*, 2019, **141**, 4130–4136.

32 W. Fan, S. B. Peh, Z. Zhang, H. Yuan, Z. Yang, Y. Wang, K. Chai and D. S. D. Zhao, *Angew. Chem., Int. Ed.*, 2021, **60**, 17338–17343.

33 J. Lee, C. Y. Chuah, J. Kim, Y. Kim, N. Ko, Y. Seo, K. Kim, T. H. Bae and E. Lee, *Angew. Chem., Int. Ed.*, 2018, **57**, 7869–7873.

34 X. Mu, Y. Xue, M. Hu, P. Zhang, Y. Wang, H. Li, S. Li and Q.-G. Zhai, *Chin. Chem. Lett.*, 2023, **34**, 107296.

35 C. Jiang, C. Hao, X. Wang, H. Liu, X. Wei, H. Xu, Z. Wang, Y. Ouyang, W. Guo, F. Dai and D. Sun, *Chem. Eng. J.*, 2023, **453**, 139713.

36 L. Yang, W. Xie, Q. Fu, L. Yan, S. Zhang, H. Jiang, L. Li, X. Gu, D. Liu, P. Dai, Q. Zheng and X. Zhao, *Adsorpt. Sci. Technol.*, 2023, **2023**, 4740672.

37 J. Zhang, Y.-Y. Xue, P. Zhang, H.-P. Li, Y. Wang, J. Xu, S.-N. Li and Q.-G. Zhai, *Cryst. Growth Des.*, 2022, **22**, 469–477.

38 W. He, X.-B. Mu, J. Lei, W. Yuan, P. Zhang and Q.-G. Zhai, *Cryst. Growth Des.*, 2023, **23**(6), 4346–4356.

39 S. Zou, Z. Di, H. Li, Y. Liu, Z. Ji, H. Li, C. Chen, M. Wu and M. Hong, *Inorg. Chem.*, 2022, **61**, 7530–7536.

40 Z. Huang, K. Chai, C. Kang, R. Krishna and Z. Zhang, *Nano Res.*, 2023, **16**, 7742–7748.

41 J. Wang, Y. Zhang, P. Zhang, J. Hu, R.-B. Lin, Q. Deng, Z. Zeng, H. Xing, S. Deng and B. Chen, *J. Am. Chem. Soc.*, 2020, **142**, 9744–9751.

42 R.-B. Lin, L. Li, H. Wu, H. Arman, B. Li, R.-G. Lin, W. Zhou and B. Chen, *J. Am. Chem. Soc.*, 2017, **139**, 8022–8028.

43 J. Li, L. Jiang, S. Chen, A. Kirchon, B. Li, Y. Li and H.-C. Zhou, *J. Am. Chem. Soc.*, 2019, **141**, 3807–3811.

